



Preclinical evaluation of [¹¹C]GW457427 as a tracer for neutrophil elastase



Sergio Estrada ^a, Mathias Elgland ^{a,b}, Ram Kumar Selvaraju ^a, Kevin Mani ^c, Gustaf Tegler ^c, Anders Wanhainen ^c, Dick Wågsäter ^d, Mats Bergström ^e, Pilar Jimenez-Royo ^e, Mahabuba Jahan ^{a,b}, Patrik Nordeman ^{a,b}, Gunnar Antoni ^{a,b,*}

^a Department of Medicinal Chemistry, Uppsala University, Uppsala, Sweden

^b PET Centre, Centre for Medical Imaging, Uppsala University Hospital, Uppsala, Sweden

^c Department of Surgical Sciences, Uppsala University, Uppsala, Sweden

^d Department of Medical Cell Biology, Uppsala University, Uppsala, Sweden

^e GlaxoSmithKline, Clinical Imaging, UK

ARTICLE INFO

Article history:

Received 25 November 2021

Received in revised form 22 December 2021

Accepted 3 January 2022

Keywords:

Neutrophil elastase

PET

Immuno-inflammation

Preclinical-PET

ABSTRACT

Introduction: Neutrophils are part of the innate immune system and function as a first line of defense against invading microorganisms. Overactivity of the immune system may result in a devastating immuno-inflammation with extensive damage to tissue leading to organ damage and/or failure. The literature suggests several human diseases in which neutrophil elastase (NE) is postulated to be important in the pathophysiology including inflammatory bowel disease (IBD), chronic obstructive pulmonary disorder (COPD), abdominal aortic aneurysms (AAA), breast and lung cancer, and recently also in Sars-cov-2 virus infection (Covid-19). In particular, the lungs are affected by the destructive power of the protease neutrophil elastase (NE). In this paper, we report the pre-clinical development of a selective and specific positron emission tomography (PET) tracer, [¹¹C]GW457427, as an *in vivo* biomarker for the study of NE, now available for human studies.

Methods: [¹¹C]GW457427 was produced by methylation of GW447631 using [¹¹C]methyl triflate and GMP validated production and quality control methods were developed. Chemical purity was high with no traces of the precursor GW611437 or other uv-absorbing compounds. A method for the determination of intact [¹¹C]GW457427 in plasma was developed and the binding characteristics were evaluated *in vitro* and *in vivo*. An animal model for lung inflammation was used to investigate the specificity and sensitivity of the [¹¹C]GW457427 tracer for neutrophil elastase (NE) in pulmonary inflammation, verified by blockade using two structurally different elastase inhibitors.

Results: [¹¹C]GW457427 was obtained in approximately 45% radiochemical yield and with a radiochemical purity higher than 98%. Molar activity was in the range 130–360 GBq/μmol. Binding to NE was shown to be highly specific both *in vitro* and *in vivo* and a significantly higher uptake of tracer was found in a lipopolysaccharide mouse model of pulmonary inflammation compared with control animals. The uptake in lung tissue measured as standardized uptake value (SUV) strongly correlated with tissue NE content as measured by ELISA. *In vitro* studies also showed specific tracer binding in aortic tissue of patients with abdominal aorta aneurysm (AAA). The rate of metabolism in rats was appropriate considering the critical balance between available tracer for binding and requirement for blood clearance with about 40% and 20% intact [¹¹C]GW457427 in plasma at 5 and 40 min, respectively. Radioactivity was cleared from blood and organs in control animals with mainly hepatobiliary excretion with distribution in the intestines and the urinary bladder; but without retention of the tracer in healthy organs of interests such as the lung, liver, kidneys or in the cardiovascular system. A dosimetry study in rat indicated that the whole-body effective dose was 2.2 μSv/MBq with bone marrow as the limiting organ. It is estimated that up to five PET-CT investigations could be performed in humans without exceeding a total dose of 10 mSv.

Conclusion: [¹¹C]GW457427 is a promising *in vivo* PET-biomarker for NE with high specific binding demonstrated both *in vitro* and *in vivo*. A GMP validated production method including quality control has been developed and a microdosing toxicity study performed with no adverse signs. [¹¹C]GW457427 is currently being evaluated in a First-In-Man PET study.

© 2022 The Authors. Published by Elsevier Inc. This is an open access article under the CC BY license (<http://creativecommons.org/licenses/by/4.0/>).

* Corresponding author at: PET Center, Uppsala University Hospital, SE-751 85 Uppsala, Sweden.
E-mail address: gunnar.antoni@akademiska.se (G. Antoni).

1. Introduction

Inflammatory reactions as primary or secondary phenomena are involved in most of human diseases. The pathological representations of inflammation include many different aspects of tissue reactions such as chronic upregulation of proteolytic enzymes, fibrinogenic cytokines, angiogenic factors, growth factors as well as autoimmune responses. In this process immune active cells, such as leukocytes play a key role.

Neutrophils are the most abundant leukocytes in the circulation. They are part of the innate immune system acting as first line of defense in the immune response and found in many inflammatory diseases, notably in inflammatory bowel disease (IBD) mainly ulcerative colitis (UC) and lung diseases like cystic fibrosis (CF), bronchiectasis (BE) and chronic obstructive pulmonary disease (COPD). Whilst abdominal aortic aneurysm (AAA) is not regarded primarily as an inflammatory disease, involvement of inflammatory cells in the destruction of elastin in the vessel wall is the primary driver of aneurysm formation [1–7].

Neutrophils are also known to be involved in the devastating immuno-inflammation found in Acute Respiratory Distress Syndrome (ARDS) and furthermore, it was recently hypothesized that the same mechanism could be responsible in the secondary COVID-19 pulmonary inflammation [8,9].

The defense mechanism of neutrophils consists of the three following modes of action; phagocytosis, degranulation and NETosis with the release of nuclear material in the form of neutrophil extracellular traps (NETs) [10]. Neutrophils also promote recruitment of additional neutrophils, dendritic cells, monocytes and lymphocytes into the tissue creating a vicious self-amplifying cycle leading to chronic immuno-inflammation and subsequent development of fibrosis through interactions with fibroblasts. A key event of neutrophil activity is the release of the protease neutrophil elastase (NE) *via* degranulation of azurophilic granules creating a high local concentration of NE, either bound to the outer cell membrane of the neutrophils or in the form of NETs. A key purpose of NE is to degrade components of the extracellular matrix, for example elastin, thereby allowing granulocytes and macrophages to traverse tissue and reach sites of inflammation. NE also cleave the pre-formed proteins into pharmacologically active signaling peptides which act as regulators of cellular function promoting chemotaxis of other immune cells to the inflamed tissue. This overactive immune response may exacerbate the patient's condition and worsen the outcome of infection. The proteolytic activity of NE is balanced *in vivo* by the antiprotease α 1-antitrypsin. It is well established that α 1-antitrypsin deficiency leads to an imbalance of protease/antiprotease with a subsequent destruction of lung tissue [11].

Neutrophil elastase has been a target for drug development in pulmonary disease with therapies aiming to protect lung tissue. Several drugs have been investigated in clinical trials, for example Sivelestat® and AZD9668, with mixed results and no conclusive evidence of efficacy although some positive results are reported [2,12,13]. In these studies no molecular imaging modality, such as positron emission tomography (PET), was used to investigate the *in vivo* interaction between drug and NE and it can be hypothesized that the lack of clinical efficacy either was due to too short treatment period or too low dose. The latter is a plausible explanation considering the very high local concentration of NE in tissue.

In AAA, elastase activity contributes to elastin degradation and aneurysm formation throughout disease progression. Elastase inhibition has been shown to reduce aneurysm growth in relevant animal models but at present, no medical therapies, established or in development are available that can halt aneurysm expansion in patients [14]. Although functional imaging of AAA patients suggests that inflammation in the aortic wall contributes to its degradation [15], these results are inconclusive; furthermore, the degree of elastase activity in the vessel wall cannot be quantified with [18 F]fluorodeoxy glucose (FDG), being a more generic marker of inflammation that records increased glucose uptake [16, 17]. It's clearly important to increase our understanding of the complex

interplay between cytokine signaling and microenvironmental factors and how these influence the inflammatory responses of neutrophils. Thus, our current knowledge is insufficient to fully understand immuno-inflammation and specifically the role of NE. Furthermore, there are several potential exploratory therapeutic interventions that can be identified and studied by applying molecular imaging targeting NE. The concentration of elastase in the azurophilic granules is high (about 5–10 mM) which leads to significant local concentration of the protease upon release, enough to be measured with a selective and specific PET-radioligand. For this purpose, we have developed [11 C]GW457427 (coined [11 C]NES) as a selective and specific PET-tracer for the study of neutrophil elastase *in vivo* in humans using PET, here validated *in vitro* in human abdominal aortic aneurysm tissue compared with healthy aorta and *in vivo* in a lipopolysaccharide animal model of lung inflammation compared with control animals. We also present a GMP validated production method and toxicology data for [11 C]GW457427.

2. Material and methods

2.1. General

For details see supporting information.

2.2. Radiochemistry

[11 C]GW457427, (3S,3aS,6aR)-4-(5-((cyclopropylamino)methyl)pyrazine-2-carbonyl)-3-isopropyl-1-(methylsulfonyl)hexahydropyrrolo[3,2-*b*]pyrrol-2(1H)-one, (NES) was synthesized by alkylation of the corresponding desmethyl compound GW447631, (3S,3aS,6aR)-4-(5-(cyclopropylamino)pyrazine-2-carbonyl)-3-isopropyl-1-(methylsulfonyl)hexahydropyrrolo[3,2-*b*]pyrrol-2(1H)-one (1 mg) in 300 μ L of acetone using [11 C]methyl triflate (Scheme 1). When all activity had been transferred, the vial was kept at 25 °C for 1 min. The crude reaction mixture was then diluted with water and purified by semi-preparative HPLC. The solvent was removed by evaporation and the product reconstituted in phosphate buffer/saline pH 7.4 with 9% ethanol (v/v). The final solution of [11 C]GW457427 was passed through a 0.22 μ m filter into a sterile injection vial.

2.3. Validation of [11 C]GW457427 for clinical use

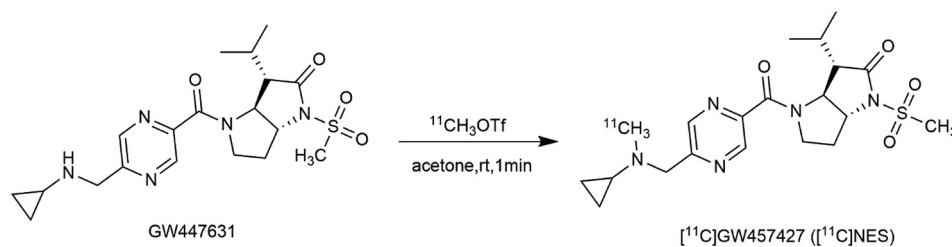
The production and quality control methods for [11 C]GW457427 were validated according to cGMP and the product specifications were based on the European Pharmacopoeia. The production process followed the flow scheme in Fig. 1.

[11 C]GW457427 was dissolved in the formulation solution immediately after removal of the HPLC eluent and subsequently passed through a 0.22 μ m filter into a sterile injection vial. A quality control sample was taken, and the volume of the product solution determined by weighing the vial and the total radioactivity of the product was measured in an ionization chamber. The release procedure follows the concept of parametric release with batch specific analyses and selected analyses performed at specified intervals, typically 10% of delivered batches. The batch quality control consisted of determination of identity, radiochemical and chemical purity and pH.

A dosimetry study was performed in rats (see Section 2.6) and the toxicology of GW457427 was investigated according to the microdosing concept (see supplementary information) [18].

2.4. Preclinical studies

Approval by the local Ethics Committee for Animal Research was obtained for all *in vivo* experiments in mice and rats, 5.8.18-01978/2018. All experiments were performed in accordance with the respective national Animal Welfare Agency guidelines and reviewed and approved



Scheme 1. Depicting the ^{11}C -methylation of precursor GW447631 yielding $^{11}\text{C}[\text{GW}457427$ ($^{11}\text{C}[\text{NES}]$).

by the GlaxoSmithKline Institutional Animal Care and Use Committee (IACUC). Human tissue was obtained from Uppsala Biobank, 2007/052 and amendment 2009/371.

The human biological samples were sourced ethically, and their research use was in accord with the terms of the informed consents under an IRB/EC approved protocol.

2.5. Metabolite analysis of [^{11}C]GW457427 in rats

Metabolite analysis was performed on blood plasma and lung tissue from Sprague-Dawley rats taken at different time points after administration of [^{11}C]GW457427 and the samples analyzed using reversed phase high performance liquid chromatography connected to a radioactivity detector (Radiomatic 610TR, Packard, USA).

[^{11}C]GW457427 (~50 MBq) was administered *i.v.* to two rats and the animals were terminated after 5, 25 or 40 min and a terminal blood sample taken. Lung tissue was taken from the rat terminated at 5 min following injection of [^{11}C]GW457427. The tissue and blood samples were prepared as described in the Supporting Information section.

2.6. Frozen section autoradiography

Snap-frozen tissues were used, including lungs of BALB/c mice with LPS induced lung inflammation and control mice as well as tumor and

spleen tissue from a subcutaneous tumor model (EMT-6). Human tissue was obtained from 10 patients (30% female) (mean age 73.9, range 72–76) who had open surgical repair for asymptomatic AAA (mean diameter 62, range 53–80). Non-aneurysmal aortic tissue samples were collected from ten organ donors (40% female) (mean age 70.2, range 66–76), at the time of explant. The AAA samples, 10 by 40 mm, were obtained from the anterior wall of the aneurysms, whereas the entire circumference of the aorta was obtained from the organ donors. The human tissue samples were covered with Tissue-Tek® OCT™, snap frozen in isopentane/dry ice and then stored at -80°C . Specimens for autoradiography were prepared from the frozen tissue by slicing 20 μm sections in a cryostat microtome (Micron HM560, Germany); the slides were mounted on Menzel Super Frost plus glass slides, dried at room temperature (RT) and stored at -20°C until used in the study. On the day of the experiments, the tissue sections were pre-incubated for 10 min at room temperature (RT) in phosphate buffered saline buffer, pH 7.4, PBS buffer. Duplicate slides were incubated in 0.1 MBq/mL [^{11}C]GW457427 for 40 min, in the presence or absence of an excess of the selective NE inhibitors, Sivelestat® (23 $\mu\text{mol/L}$) or GW311616A (2.3 $\mu\text{mol/L}$) to block the specific binding of the tracer. After incubation, slides were washed for 3×1.5 min in cold PBS buffer, followed by rapid immersion in water. Slides were then dried for 10 min at 37°C and exposed to phosphor image (PI) plates (Amersham) for >1 h, together with a 20 μL aliquot of the incubation solutions, for later quantification purposes. The PI plates were, thereafter, scanned in a phosphor imager (Amersham Typhoon IP, GE Healthcare) and the digital autoradiograms were analyzed in ImageJ (ImageJ 1.45S, NIH, Bethesda, USA). Regions of interest (ROIs) were drawn manually on the digital images and the pixel intensities were transformed to amount of radioligand using the 20 μL reference spots. Binding was calculated as total (tracer alone), non-specific (tracer in the presence of excess of competing ligand) and specific (non-specific subtracted from total) and presented as amount of bound radioligand.

2.7. ELISA measurement of total neutrophil elastase in lung tissue

A commercially available ELISA kit for determination of murine neutrophil elastase was used (Mouse Neutrophil Elastase SimpleStep ELISA Kit, Abcam Netherlands), according to the manufacturer's instructions. In brief, pieces of snap-frozen lung tissues from LPS-treated and control mice, were weighed, homogenized in a Dounce homogenizer of ice-cold cell extraction buffer (Abcam), in a volume corresponding to five times the weight of each lung piece. After incubation on ice for 20 min, the homogenates were centrifuged at 18,000 $\times g$ for 20 min, at 4°C ; the supernatants were then collected, aliquoted and snap-frozen, at -80°C , until used. Before running the ELISA assay, lung homogenate samples were diluted 1000 times to avoid exceeding the measurable range of the assay. For quantification purposes, a standard curve was determined in the same assay, with purified mouse neutrophil elastase (Abcam), in a concentration range from 78 to 5000 pg/mL . The concentration of NE in lung samples was determined by interpolating their absorbance values against the standard curve and by multiplying the resulting values by the appropriate sample dilution factor.

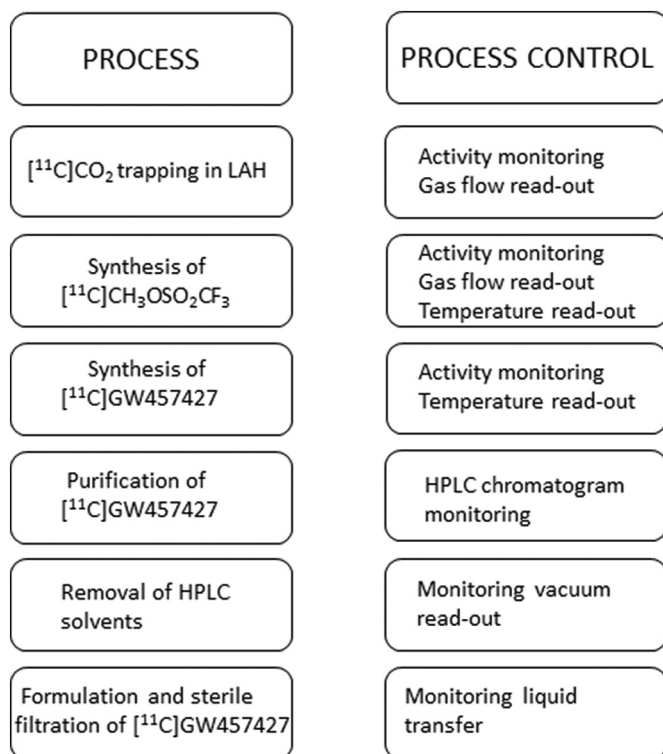


Fig. 1. Flow scheme of the production process for [^{11}C]GW457427.

2.8. Organ distribution and dosimetry in healthy rats

Eight male (396 ± 29 g) and eight female (247 ± 29 g) Sprague-Dawley rats were injected via the tail vein with [^{11}C]GW457427, 3.2 ± 0.3 MBq (male) and 3.9 ± 0.7 MBq (female) in ~ 500 μL saline. Two rats of each gender were euthanized by high concentration CO_2 , at four predetermined time points: 5, 10, 20, and 40 min post injection (p.i.), respectively. Organs were immediately extracted, their radioactivity measured in a well-type NaI (TI) scintillation counter, correction for dead-time was applied and weight was determined. The investigated organs were blood, heart, lung, liver, pancreas, spleen, adrenal, kidney, small intestine (without its content), large intestine (with its content), urinary bladder, testis/ovary, muscle, bone, site of injection and brain. The remaining carcass was also measured to monitor the radioactivity elimination and recovery. The radioactivity readings were decay-corrected to the time of the injection, and the results were expressed as standardized uptake values (SUVs) (Eq. (1)).

$$\text{SUV} \left(\frac{1}{1} \right) = \frac{\text{Radioactivity}_{\text{tissue}} (\text{Bq}) / \text{Weight}_{\text{tissue}} (\text{g})}{\text{Radioactivity}_{\text{injected}} (\text{Bq}) / \text{Weight}_{\text{body}} (\text{g})} \quad (1)$$

The SUV data from rat was extrapolated to the human species by assuming similar SUVs in human as in rat. The SUV values in rat were first multiplied with the appropriate decay factor dependent on the time point of the data post-injection, then multiplied by standard organ masses and divided by the standard total-body weight for the standard adult (male & female) phantom obtained from the OLINDA/EXM 1.1 software (Organ Level Internal Dose Assessment Code, Vanderbilt University, USA, 2007). The values obtained correspond to the fraction of injected radioactivity (%IA) per organ in man as a function of time. The %IA curve for each organ was then integrated using the trapezoid method where a simple exponential decay was assumed to occur from the last data point to eternity (as if there was no further biological decay, but only physical decay), which is a conservative approach. Bone marrow residence times were assessed according to the bone marrow blood model [19]. The absorbed dose was estimated by the OLINDA/EXM 1.1 software where the calculations were based on the adult reference male or female phantom to acquire the intended absorbed dose estimate in human organs.

2.9. LPS induced acute lung inflammation in mice

The murine lung inflammation model, which results on large recruitment and activation of neutrophils, was adapted from Corteling et al. [20] In brief, female BALB/c mice (20–25 g) were lightly sedated with 3–4% sevoflurane (Baxter, Baxter Medical AB, Kista, Sweden). After 10–30 s, when showing signs of recovering from anesthesia, mice were given an intranasal administration of 0.5 mg/kg of Lipopolysaccharide, LPS, (Salmonella Tryphosa, Sigma) in a volume of 20–25 μL (depending on body weight) and allowed to return to their cages, under observation. After 24 ± 6 h, the mice were given an intranasal administration of 0.5 mg/kg of *N*-Formylmethionyl-leucyl-phenylalanine, fMLP, (Sigma) in a volume of 20–25 μL (depending on body weight) and allowed to return to their cages, under observation. After another 5 ± 3 h, the mice were used for *in vivo* evaluation with [^{11}C]GW457427.

2.10. EMT-6 tumor model

One vial of EMT 6 cells, a murine carcinoma cell line, (ATCC: CRL-2755) (P6) was thawed from -140 $^{\circ}\text{C}$ and plated in Weymouth's MB 752/1 with 15% FBS. Cells were sub-cultured 3 times over 8 days. Trypsin/EDTA was used to facilitate cell detachment from culture flask during sub culturing. Cells were collected, washed twice, and resuspended in PBS at 1×10^6 cells/mL.

Six-week-old female BALB/cAnNHsd mice from Envigo (Frederick, MD) were used for these studies. Mice were chipped subcutaneously with BMDS IMI1000 identification microchips (Seaford, DE) and the right hind flank was shaved for clear tumor observation and treatment.

Exponentially growing EMT 6 cells were detached from flasks as described above, and 0.5 mL of cell suspension was added to a sample cup. Cell number was determined by the Vi-Cell XR Cell Viability Analyzer 2.03 (Beckman Coulter, Brea, CA), which uses trypan blue to evaluate cell viability. Cells were centrifuged (1500 rpm for 5 min at 4 $^{\circ}\text{C}$) to remove the trypsin solution. A single cell suspension was created in so that a 100 μL injection would deliver 1×10^5 cells per mouse. Tumors were established approximately (7–8 days) after injection.

2.11. Ex vivo organ distribution and in vivo PET examinations in mice

[^{11}C]GW457427, 2–5 MBq, in saline, was administered intravenously (i.v.) as a bolus to three groups of BALB/c mice: (i) animals with induced inflammation ($n = 8$), (baseline group); (ii) animals with induced inflammation ($n = 6$), which also received a co-injection of excess of unlabelled GW457427 (1 mg/kg) (blocked group) and (iii) untreated BALB/c mice ($n = 6$, control group). After 40 min, the animals were euthanized and the radioactivity of the excised organs was measured, as described above. The organs selected were blood, lungs, liver, kidney, small intestine without its content, spleen and knee joint.

After measurement of organ radioactivity, the lungs were immediately snap frozen and stored at -80 $^{\circ}\text{C}$ for subsequent *in vitro* measurements.

For *ex vivo* assessment of the kinetics of tracer distribution in blood, plasma and lungs additional mice ($n = 12$), from each of the three groups described above (baseline, blocked and control), were euthanized at 3, 10, 20 and 40 min p.i., (i.e., $n = 3$ per time point) with lung tissue and terminal blood sampling collected. Radioactivity and weight of the organs were measured, and tracer uptake was calculated as described above under metabolite analysis.

In vivo dynamic PET imaging was performed in two animals from each group ($n = 6$), followed by a CT scan. Mice were positioned in a heated bed of the PET scanner (Nanoscan PET-3TMRI, Mediso, Medical Imaging Systems, Budapest, Hungary) and a dynamic PET acquisition was initiated immediately before injection of [^{11}C]GW457427. The duration of the PET scan was 40 min, with the thorax in the field of view. After the PET acquisition, the bed was transferred to a preclinical SPECT/CT (Nanoscan SPECT (4H)-CT, Mediso, Medical Imaging Systems, Budapest, Hungary). A whole-body CT scan was then performed for 8 min. PET images from the Mediso system were reconstructed using a Tera-TomoTM 3D algorithm (Nucline 3.04.010.000; Mediso Medical Imaging Systems, Budapest, Hungary) with 4 iterations and 6 subsets. PET-CT images were fused and analyzed in PMOD 4.0 (PMOD Technologies, Zürich, Switzerland).

3. Results and discussion

3.1. Radiochemistry

The production of [^{11}C]GW457427 was set up in a GMP-compliant manner on our semi-automatic in-house developed Tracer Production System (TPS). The desmethyl cyclopropyl amine precursor GW447631 (1.0 mg) dissolved in 300 μL acetone was readily ^{11}C -methylated using [^{11}C]methyl triflate at 25 $^{\circ}\text{C}$ for 1 min (Scheme 1) in nearly quantitative yield. A typical synthesis took about 40 min from end of bombardment and provided [^{11}C]GW457427 in a reproducible radioactivity yield of 5.7–7 GBq. The radiochemical yield based on an approximate starting amount of 50 GBq [^{11}C]carbon dioxide was estimated to be around 45%. The molar activity of [^{11}C]GW457478 was in the range 130–360 GBq/ μmol and radiochemical purity higher than 98%. The chemical purity was high with no traces of the precursor GW447631

and absence of unknown UV-absorbing compounds. The total production required about 50 min including quality control and release process.

3.2. GMP validation, dosimetry and toxicology studies

3.2.1. GMP validation

The production process including the QC-methods was validated according to internal standard operating procedures and documented as an Investigational Medicinal Product Dossier (IMPD). Batches of [^{11}C]GW457427 for injection will meet the following specifications (Table 1).

3.3. Microdosing toxicology study

A single dose study of GW457427 was performed by Charles River Laboratories Den Bosch BV according to the microdosing concept in Wistar Han rats with a 14-Day recovery period according to Good Laboratory Practise (GLP). The Administration of GW457427 by a single intravenous injection was well tolerated in male and female rats at dose levels of 0.143, 0.715 and 1.43 mg/kg. The latter is equivalent with a

dose 1000 times the maximum dose in humans (calculated as $\mu\text{g}/\text{kg}$ body weight), which to a 70 kg subject is equivalent to 100 μg , the maximum amount according to the microdosing concept.

No mortality occurred during the study and there were no test item-related clinical signs or effects on body weight, food consumption, clinical pathology, gross pathology, organ weights and histopathology after a single administration of up to 1.43 mg/kg and after a 14-day recovery period; other than histologic changes at the injection site that can be expected after intravenous administration.

3.4. Organ distribution and dosimetry in healthy rats

Ex vivo organ distribution data from 17 organs is presented as decay-corrected SUV values (Fig. 2).

The estimated, extrapolated radiation doses and annual dose limit to different organs are presented in Fig. 3.

The organ that showed the highest radiation dose was red bone marrow, with 3.7 $\mu\text{Sv}/\text{MBq}$ in females and 5.0 $\mu\text{Sv}/\text{MBq}$ in males, while all other organs received doses lower than 1 $\mu\text{Sv}/\text{MBq}$, in both genders. The high uptake of [^{11}C]GW457427 in red bone marrow fits well with the fact that neutrophils are produced and stored in this organ and contain high density of neutrophil elastase in the azurophilic granules.

The whole-body effective radiation dose for [^{11}C]GW457427 was 2.2 $\mu\text{Sv}/\text{MBq}$, for both genders, which would allow for administration of >4500 MBq per year to healthy volunteers (before reaching 10 mSv/year).

Table 1

Release and quality specifications for [^{11}C]GW457427 injection.

Test parameter	Method	Specification
SST	HPLC	SST chromatogram corresponds to the reference chromatogram
Identity	HPLC	The retention time of product radio peak and the reference UV peak matches (± 1 min adjusted for measured difference between the UV and the radioactivity detector)
GW447631	HPLC	<5 $\mu\text{g}/\text{mL}$
Chemical purity	HPLC	No unidentified peaks in the UV chromatogram compared to the reference chromatograms.
Radiochemical purity	HPLC	$\geq 90\%$, no single impurity larger than 5%
pH	pH paper	4–8
Filter integrity	Bubble point	≥ 3450 mbar
Appearance	Visual inspection	Colorless and particle free
Volume	Volume determined by weight	6–7 mL
Radioactivity	Dose calibrator	In relation to volume, see limit in radioactivity concentration
Radioactivity concentration	Dose calibrator/volume	Not more than 800 MBq/mL
Tests performed on selected batches		
Sterility ^a	Ph. Eur. 2.6.1	No anaerobic and aerobic bacterial growth
Endotoxins ^a	Ph. Eur. 2.6.14	≤ 0.25 EU/mL
Bioburden ^b	Ph. Eur. 2.6.12	Microbial Enumeration test on unfiltered formulated product ≤ 10 CFU/mL
^c Radionuclidic purity	Spectroscopy	>99%
^d Radionuclide identity	Approximate half-life determination	According to the pharmacopoeia (20.35 min $\pm 10\%$)
Residual solvents ^a		
Acetonitrile	GC	≤ 410 ppm
Acetone	GC	≤ 5000 ppm
Methanol	GC	≤ 3000 ppm
Tetrahydrofuran	GC	≤ 720 ppm
Ethanol (Excipient)	GC	$\leq 10\%$

^a Approximately every 10th production batch is sampled, and results are available after the product has expired.

^b Test performed twice yearly on [^{11}C]GW457427 or other product manufactured using the same equipment.

^c When change of target holder is performed.

^d The identity of the product is specified as [^{11}C]GW457427 and the analysis for identity also specifies the radionuclide.

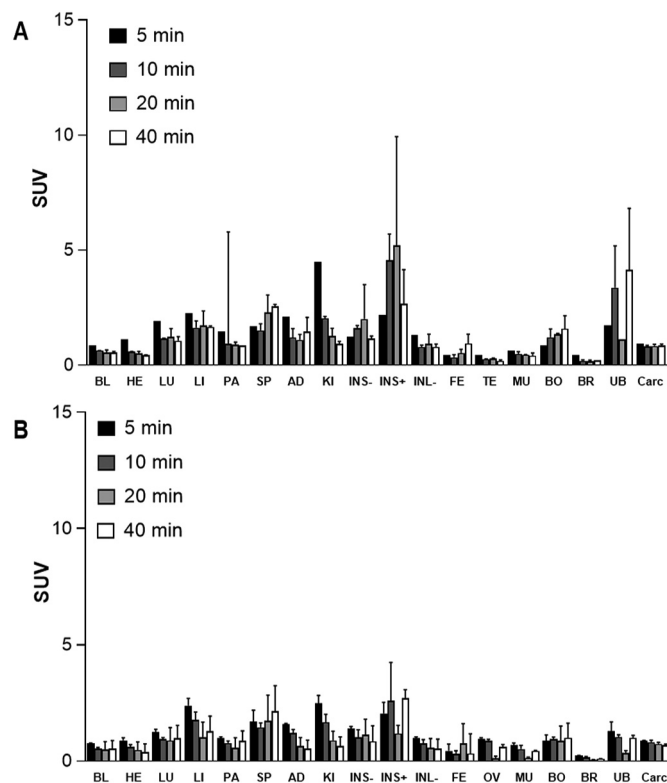


Fig. 2. Uptake of [^{11}C]GW457427 in different organs assessed by *ex vivo* biodistribution in male (A) and female (B) rats. At each time point, two animals of each gender were used. Tracer distribution was estimated at 5-, 10-, 20- and 40-minutes post injection. The tracer was rapidly cleared from blood to tissues (SUV in blood was below one, 5 min post injection). SUV values were recorded as follows at 40 min post injection: small intestine with contents (2.7 ± 1.5 , males; 2.7 ± 0.4 , females), liver (1.6 ± 0.04 , males; 1.3 ± 0.7 , females), kidneys (0.9 ± 0.1 , males; 0.7 ± 0.4 , females). Organs abbreviation: BL- Blood, HE-Heart, LU-Lungs, LI- Liver, PA-Pancreas, SP-Spleen, AD-Adrenal glands, KI-Kidney, INS(-) - small intestine without content, INS (+) -small intestine with content, INL (-) - large intestine without content, FE- faeces, TE-Testes, OV-Ovaries, MU-Muscle, BO- Bone, BR-Brain, UB-Urinary bladder, Carc- Carcass.

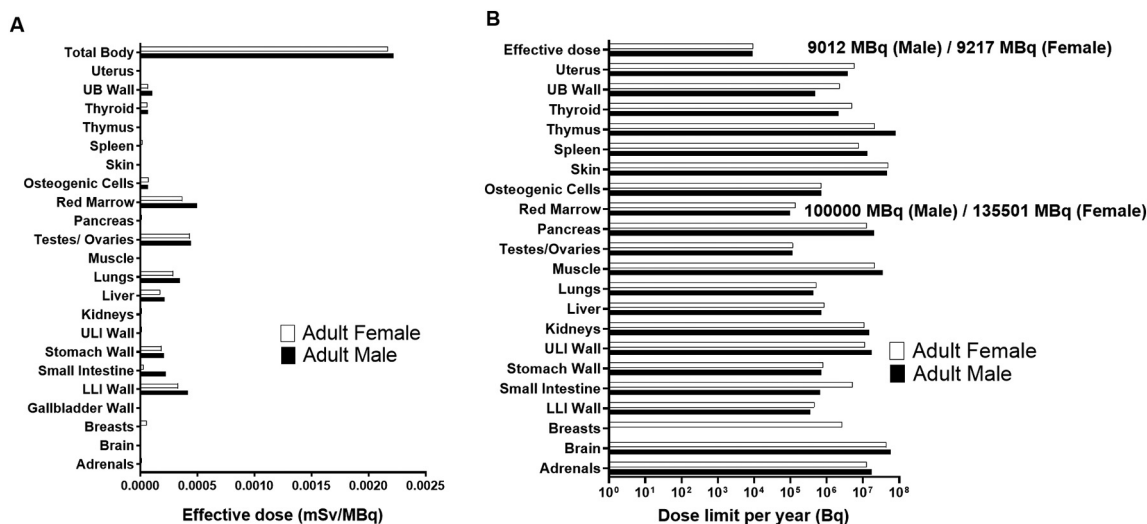


Fig. 3. Dosimetry of $[^{11}\text{C}]\text{GW457427}$. (A) The absorbed radiation dose in relevant tissues per MBq of administered $[^{11}\text{C}]\text{GW457427}$, as predicted in humans based on dynamic rat biodistribution data. (B) The acceptable radioactive dose (in MBq) of $[^{11}\text{C}]\text{GW457427}$ that can be administered per year in healthy subjects, as calculated from absorbed dose per tissue and the annual regulatory safety limit for each tissue.

It can be concluded that $[^{11}\text{C}]\text{GW457427}$ can be safely administered intravenously to human subjects at doses up to 100 μg , either as a single or multiple bolus administration.

3.5. Metabolite analysis

It was found that using acetonitrile as precipitating agent, the recovery of $[^{11}\text{C}]\text{GW457427}$ and radioactive metabolites from plasma of rats decreased with time; 5 min 83% ($n = 2$), 25 min 66% ($n = 1$), 40 min 46% ($n = 2$). We hypothesize that the decreased recovery over time in the *in vivo* experiments is most likely the result of adsorption of labelled metabolites by plasma constituents removed during centrifugation. As a control, the sample preparation recovery was determined by incubating $[^{11}\text{C}]\text{GW457427}$ in human plasma. The samples were stored at room temperature for up to 30 min and acetonitrile was used as the precipitating agent. The recovery was 94% ($n = 3$, RSD = 0.6%) indicating that the tracer is stable under these conditions. In contrast, using 7% perchloric acid as the precipitating agent resulted in a 63% ($n = 3$, RSD = 3%) recovery. Therefore, acetonitrile was selected as the precipitating agent. The radiochromatograms acquired when analyzing plasma from blood samples withdrawn at 5, 25 and 40 min, respectively revealed that the metabolites were well resolved from the parent tracer $[^{11}\text{C}]\text{GW457427}$. Metabolism is rather fast with about 38% intact tracer at 5 min, 24% at 25 min and with 17% at 40 min. In comparison, analysis of the sample prepared from lung tissue removed 5 min p.i. showed that approximately 61% of the tracer was intact. In addition, it appears as other metabolites are found in the lung compared to plasma (see supporting information) that could indicate lung tissue related metabolism. In conclusion, the developed method can be used for kinetic modeling by adjusting for the lower recovery of radiometabolites with time.

3.6. Ex vivo organ distribution and in vivo PET examinations in mice

The uptake of $[^{11}\text{C}]\text{GW457427}$, 40 min p.i., was significantly ($p = 0.0013$) higher in the lungs of mice treated with LPS/fMLP, with an SUV of 5.5 ± 2.7 , than in lungs of control mice, SUV 0.79 ± 0.06 (Fig. 3A). In treated mice, co-injected with excess of unlabeled GW457427, the uptake was significantly ($p = 0.0012$) reduced to levels similar to those in control mice, SUV 0.75 ± 0.3 , (Fig. 3A) indicating high selectivity of the tracer for tissue with elevated concentration of neutrophil elastase. For the rest of the investigated organs, uptake of $[^{11}\text{C}]\text{GW457427}$ was low, and unaffected by treatment and/or blocking; the exception being

the spleen, which showed higher uptake in treated than in untreated mice ($p = 0.031$), significantly ($p = 0.0003$) decreased by co-administration of excess of GW457427.

The *ex vivo* assessment of the kinetics of tracer distribution in blood, plasma and lungs at four different time points, revealed very similar kinetics in blood and plasma, exhibiting washout kinetics; while a pronounced retention was observed in the lungs of LPS/fMLP treated mice abolished in the presence of excess of unlabelled GW457427 (Figs. 4B–D).

Dynamic PET studies were in good agreement with *ex vivo* data and similarly showed high uptake in the lungs of treated (LPS + fMLP) animals but abolished in the control and the blocked group. A direct comparison between lung-SUV values determined by PET and by *ex vivo* measurements is not possible, but, assuming a lung density of 0.3 g/mL, SUV values would have been ~6 at the end of the PET acquisition (40 min), (Figs. 5 and 6).

Dynamic PET also revealed the kinetics of uptake in other organs in mice. For control mice, this was similar to the uptake and clearance from organs in rat, obtained in the *ex vivo* dosimetry study, and showed rapid wash-out kinetics in the majority of the organs, transient accumulation in liver and kidneys, increased radioactivity in the knee joint and in the intestines suggesting hepatobiliary elimination and specific uptake in red bone marrow, where neutrophils are generated and stored (Fig. 7).

3.7. Tissue analysis: frozen section autoradiography and biochemical analysis (ELISA) of NE

In vitro autoradiography experiments revealed high and displaceable binding of $[^{11}\text{C}]\text{GW457427}$ in the lungs of the murine inflammation model (Fig. 8), compared to control lungs. Similar results were observed in the tumor and spleen tissues of the EMT-6 tumor model. In addition, aorta tissue from ten asymptomatic AAA patients and from ten controls were also studied. Specific, displaceable binding was observed in some but not all samples (Fig. 8) and the specific binding was not significantly higher in AAA than in control aortas. However, handling and preparation of the human tissue may result in losses of inflamed and fibrotic parts which potentially could have reduced the amount of NE. Most importantly is the evidence of specificity in binding of $[^{11}\text{C}]\text{GW457427}$ also to human NE.

Large variability was observed in the *in vivo* uptake of $[^{11}\text{C}]\text{GW457427}$, in lungs of mice treated with LPS + fMLP (baseline group), and to some extent in the spleen (Fig. 4A). We hypothesized

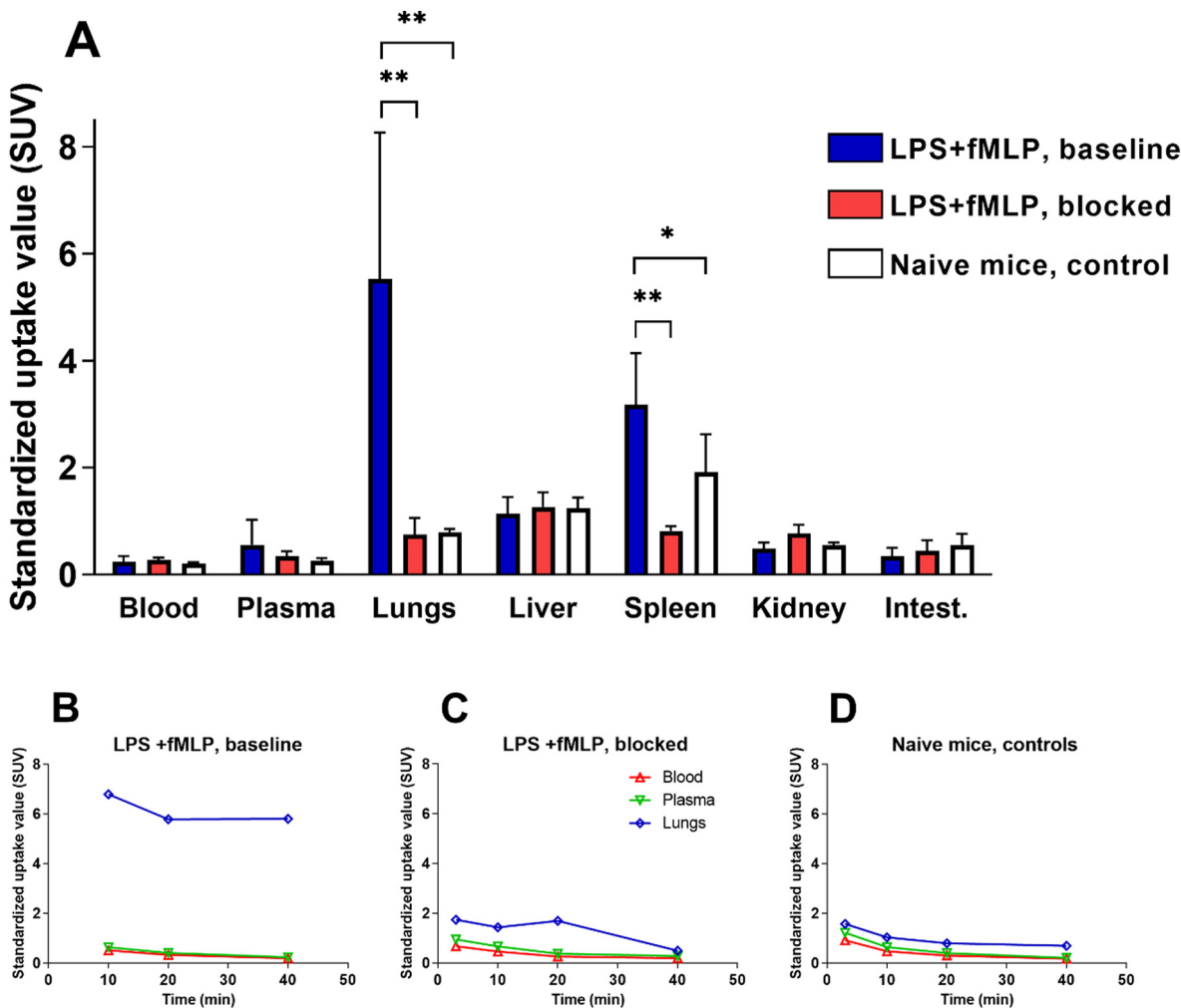


Fig. 4. Graphs, showing the results from quantitative *ex vivo* measurements of distribution of [^{11}C]GW457427 in the three groups of mice; mice with LPS induced lung inflammation injected with [^{11}C]GW457427; mice with LPS induced lung inflammation, injected with [^{11}C]GW457427 + 1 mg/kg of unlabelled GW457427 and control animals, injected with [^{11}C]GW457427. (A) Animals were euthanized 40 min p.i. and selected organs were excised and measured *ex vivo*. Significantly higher uptake was observed in lungs and spleens of mice treated with LPS + fMLP than that in control mice and in mice co-injected with 1 mg/kg of unlabelled GW457427. Graphs (B), (C) and (D) show *ex vivo* distribution of [^{11}C]GW457427 in blood, plasma and lungs, at 3-, 10-, 20- and 40-min post injection, respectively, in the three different groups.

that this variability could be due to the LPS challenge resulting in different levels of inflammation with a large variation in the levels of recruited neutrophils. Therefore, lung tissue from treated mice (LPS + fMLP, baseline group) that had showed a variation of uptake of [^{11}C]GW457427, spanning from SUV = 0.46 to SUV = 15.6, was also examined by *in vitro* autoradiography and the content of elastase in these lungs was measured by ELISA. A very good correlation ($p = 0.0029$) was obtained between *in vitro* binding of [^{11}C]GW457427 and its *in vivo* uptake, as assessed by SUV values, in mice with varying levels of inflammation, (Fig. 9A). Furthermore, the almost perfect correlation ($R^2 = 0.9953$; $p < 0.0001$) that we obtained between uptakes *in vivo* (SUV values) and amounts of NE in lung (Fig. 9B), strongly supports hypothesis. The very strong correlations suggest that *in vivo* non-invasive imaging with [^{11}C]GW457427 PET tracer is very specific for neutrophil elastase.

3.8. Summary of preclinical studies

The *in vivo* stability of [^{11}C]GW457427 recorded in rats is suitable, sufficiently long to allow binding to NE and shows rapid with clearance from non-target tissue. Autoradiography studies have demonstrated high specific binding in different tissues from animal models, typically in the range of 85–90%, and also specificity towards human NE. *In vivo*

imaging studies have revealed very low tracer uptake in healthy tissue, apart from bone marrow, with some distribution in the intestines due to hepato-biliary excretion. Small animal PET-CT-MR studies in the LPS pulmonary inflammation model in mice as described showed high uptake in lungs which could be blocked by co-injection of GW457427. The specificity in binding to elastase was confirmed *in vitro*, using the two structurally different selective elastase inhibitors, Sivelestat® and GW311616. Hence, [^{11}C]GW457427 is a very promising PET biomarker for NE and currently, it is being investigated in a First-In-man study (EudraCT No: 2020-003980-24).

4. Conclusions

[^{11}C]GW457427 ([^{11}C]NES) can be generated reproducibly according to GMP in high radiochemical yield with a radiochemical yield and radiochemical purity of 45% and > 98%, respectively. The molar activity is in the range of 130–360 GBq/ μmol and starting with about 50 GBq of [^{11}C]carbon dioxide a 5.7–7 GBq batch of [^{11}C]NES is obtained. A GMP-compatible production method, including validation of QC-methods has been established. The *in vivo* stability of [^{11}C]NES in rats is suitable. Sufficiently long to allow binding to NE and with fast clearance from blood and non-target tissue. Specific binding to NE in different tissues from animals is high, in the range of 85–90%, and specific binding to

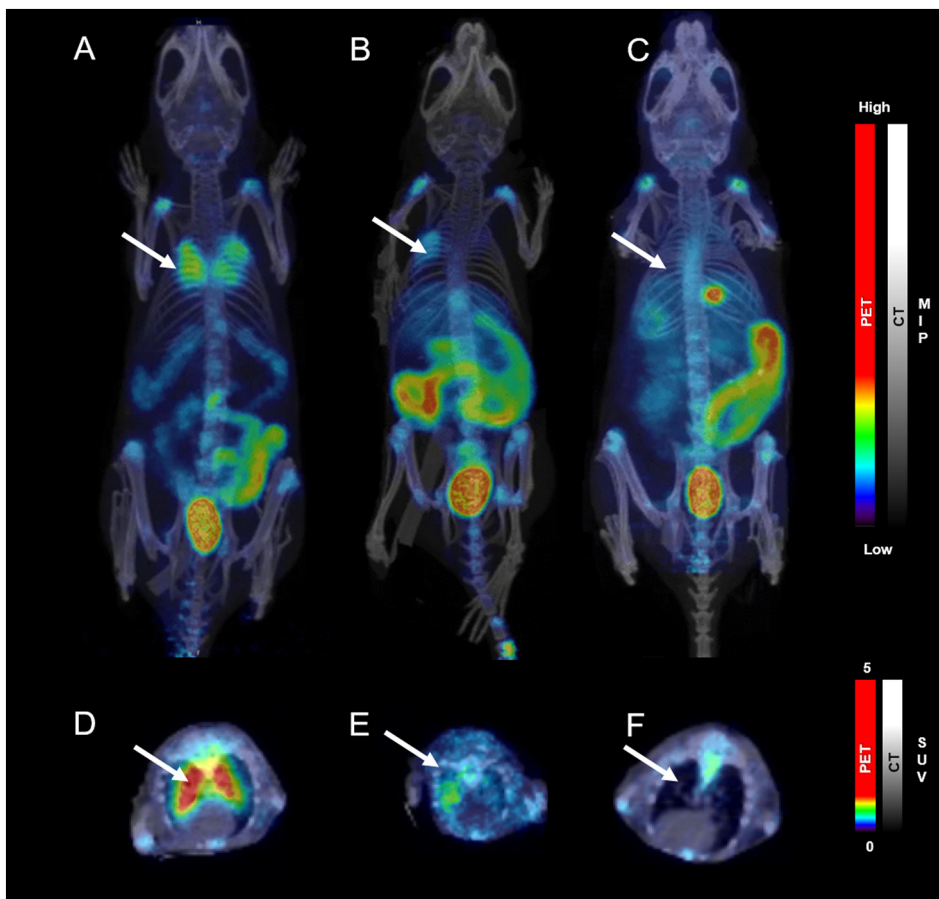


Fig. 5. Whole body PET-CT biodistribution of $[^{11}\text{C}]$ GW457427 in mice treated with LPS + fMLP at baseline (A), block (B) and control mice (C). Whole body images are a representation of the 0–40 min average, presented as maximum intensity projection (MIP). Lower row shows trans-axial view of $[^{11}\text{C}]$ GW457427 uptake in lungs of mice treated with LPS + fMLP at baseline dose (D), block (E) and control mice (F). Color scales are adjusted for SUV 5. PET images are presented in RGB color scale.

human NE established in AAA tissue from patients. Uptake of $[^{11}\text{C}]$ NES in healthy tissue is very low, apart from bone marrow, with some distribution in the intestines due to hepato-biliary excretion. Small animal PET-CT-MR studies in a LPS pulmonary inflammation model in mice showed high uptake in lungs which could be blocked. Radiation dose is low potentially allowing up to 10 administrations of a typical standard dose of radioactivity (400 MBq) with a total effective dose <10 mSv. A toxicology study using a dose 1000 times the maximum allowed dose of GW457427 administered to a human according to the microdosing

concept (100 μg) showed no sign of adverse effects. $[^{11}\text{C}]$ NES is a very promising PET biomarker for NE.

Declaration of competing interest

The authors report no conflict of interests.

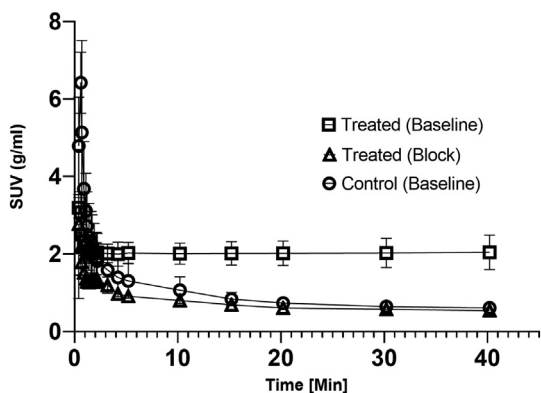


Fig. 6. Kinetic of $[^{11}\text{C}]$ GW457427 in lungs of mice models assessed by PET imaging. LPS + fMLP treated group, at baseline, clearly showed retention of tracer in inflamed lungs. However, co-injection with 1 mg/kg GW457427 showed displacement of the tracer and lung uptake at similar levels as the control group.

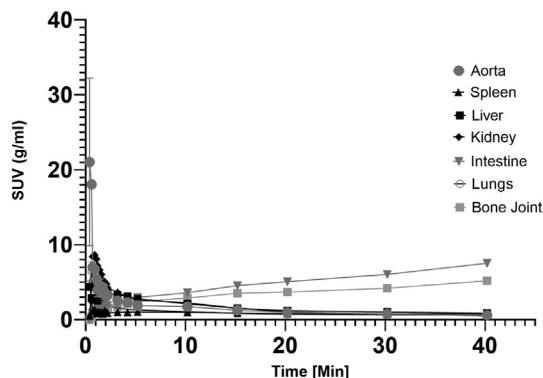


Fig. 7. Kinetic of $[^{11}\text{C}]$ GW457427 in different organs estimated from dynamic PET imaging in a control group ($n = 2$). Similar pharmacokinetics were seen to the *ex-vivo* biodistribution study in rats (Fig. 1) with fast tracer clearance from blood and accumulation in the intestine over time. Accumulation of the tracer in bone joints was observed only during imaging; this uptake was only partially displaced in the LPS + fMLP blocked cohort as shown in Fig. 5.

Sample ID	Total binding, [¹¹ C]GW457427 alone	Binding in presence of 2.3 μM of GW311616A	
909.1 AK/14			Human abdominal aorta aneurysm
9788.1 AK			
1284.1 AK/14			Human aorta, control
10579.1 AK			
Mouse#2			Mouse lung inflammation model
Mouse#7			
Mouse#3			Mouse lung, control
Mouse nr3			Mouse tumor model (EMT-6), spleen and tumor
Mouse nr4			

Fig. 8. Autoradiographs (pseudo-colored) of frozen sections with [¹¹C]GW457427 of different tissue samples including human abdominal aortas, from controls and from AAA patients; mouse lung tissue from an LPS-induced inflammation model and spleen and tumor tissue mouse from a mouse tumor model (EMT-6). Co-incubation with excess of the selective NE inhibitor GW311616A (right column) blocked tracer binding to more than 85% (in the mouse models and/or some of the aorta samples).

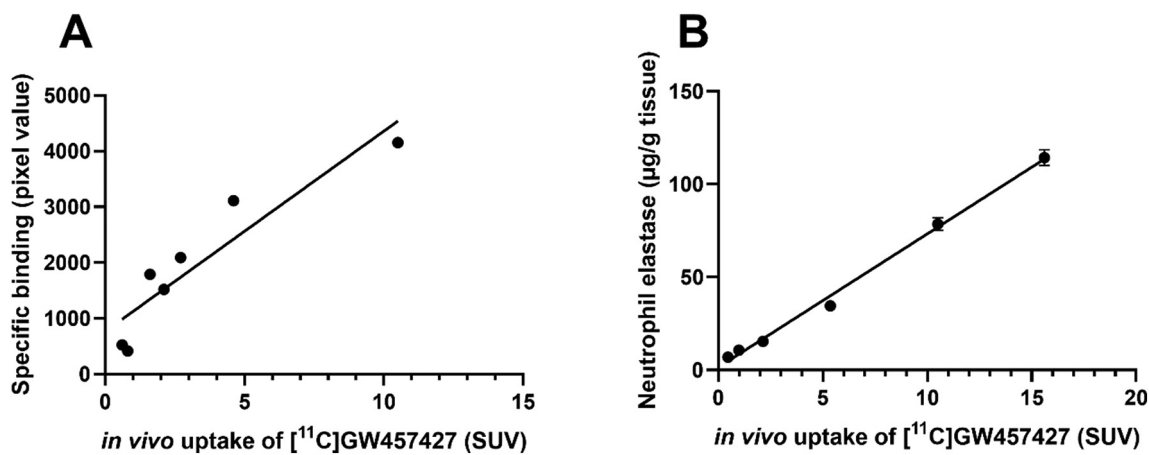


Fig. 9. Graphs showing correlations between *in vivo* uptake of [¹¹C]GW457427, presented as SUV, and two different biochemical methods of determining the amount of NE in the examined lung tissues. Correlation was analyzed only for the treated, baseline group (LPS + fMLP). (A) A very high correlation was found with *in vitro* autoradiography ($R^2 = 0.8547$; $p = 0.0029$). (B) An outstanding correlation was found with quantitative mouse neutrophil elastase as measured by ELISA ($R^2 = 0.9953$; $p < 0.0001$).

Acknowledgments

This work was financially supported by the Swedish Heart and Lung Foundation Grant 20200584. The molecular imaging work in this study was performed at the SciLifeLab Pilot Facility for Preclinical PET–MRI, a Swedish nationally available imaging platform at Uppsala University, Sweden, financed by the Knut and Alice Wallenberg Foundation.

We acknowledge the support from the EATRIS team for initiating and managing the public-private interactions and contractual aspects for this study as part of the “Immune Inflammation and Imaging Hub”. We acknowledge the initial radiochemistry work performed by Imanova Ltd.

Disclosures

This study was financially supported by GlaxoSmithKline as part of public-private collaboration executed under the EATRIS framework research agreement of the “Immune Inflammation and Imaging Hub”.

Appendix A. Supplementary data

Supplementary data to this article can be found online at <https://doi.org/10.1016/j.nucmedbio.2022.01.001>.

References

- [1] C Rosales, Front Physiol Neutrophils: a cell with many roles in inflammation or several cell types 9:113. doi: 10.3389/fphys.2018.00113
- [2] Stockley R, De Soya A, Gunawardena K, Perrett J, Forsman-Semb K, Entwistle N, Snell N. Phase II study of a neutrophil elastase inhibitor (AZD9668) in patients with bronchiectasis. *Respir Med.* 2013;107:524e533.
- [3] Keir HR, et al. Personalised anti-inflammatory therapy for bronchiectasis and cystic fibrosis: selecting patients for controlled trials of neutrophil elastase inhibition. *ERJ Open Res.* 2019. ;5 00252-2018.
- [4] Martinez-Alemán SR, et al. Understanding the entanglement: neutrophil extracellular traps (NETs) in cystic fibrosis. *Front Cell Infect Microbiol.* 2017;7:104.
- [5] Renata Curciarello R, Sobande T, Jones S, Giuffrida P, MacDonald TT, Kok K, Di Sabatino A, Guillermo H, Docena GH. Human neutrophil elastase proteolytic activity in ulcerative colitis favors the loss of function of therapeutic monoclonal antibodies. *J Inflamm Res.* 2020;13:233–43.
- [6] Thomson RW, Curci JA, Ennis TL, Mao D, Pagano MB, Pham CTN. Pathophysiology of abdominal aortic aneurysm: insight from the elastase-induced model in mice with different genetic backgrounds. *Ann N Y Acad Sci.* 2006;1085:59–73.
- [7] Cohen JR, Mandell C, Wise L. Characterization of human aortic elastase found in patients with abdominal aortic aneurysm. *Surg Gynecol Obstet.* 1987. ;165 301-301.
- [8] S-C Yang Y-F Tsai Y-L Pan T-L Hwang Understanding the role of neutrophils in acute respiratory distress syndrome. *Biomed J.* 10.1016/j.bj.2020.09.001.
- [9] Baxter-Stoltzfus A, Borczuk A, Cools-Lartigue J, Crawford JM, Daßler-Plenker J, Guerci P, Huynh C, Knight JS, Loda M, Looney MR, Rayes R, Renaud S, Rousseau S, Salvatore S, Schwartz RE, Spicer JD, Yost CC, Weber A, Zuo Y, Egeblad M, Barnes BJ, Jose M, Adrover MJ, McAllister F. Targeting potential drivers of covid-19: neutrophil extracellular traps. *J Exp Med.* 2020. ;217(6).
- [10] Brinkmann V, Reichard U, Goosmann C, Fauler B, Uhlemann Y, Weiss DS, Weinrauch Y, Zychlinsky A. Neutrophil extracellular traps kill bacteria. *Science.* 2004;303:1532–5.
- [11] McCarthy C, Reeves EP, McElvaney NG. The role of neutrophils in Alpha-1 antitrypsin deficiency. *Ann Am Thorac Soc.* 2016 Aug;13(Suppl 4):S297–304. <https://doi.org/10.1513/AnnalsATS.201509-634KV>. PMID: 27564664.
- [12] Zeiher BG, Matuska S, Kawabat K, Repine JE. Neutrophil elastase and acute lung injury: prospects for sivelestat and other neutrophil elastase inhibitors as therapeutics. *Crit Care Med.* 2002;30(5 Suppl):S281–7.
- [13] Aikawa N, Kawasaki Y. Clinical utility of the neutrophil elastase inhibitor sivelestat for the treatment of acute respiratory distress syndrome. *Ther Clin Risk Manag.* 2014;10:621–9.
- [14] Golledge J, Moxon JV, Singh TP, Bown MJ, Mani K, Wanhainen A. Lack of an effective drug therapy for abdominal aortic aneurysm. *J Intern Med.* 2020;288:6–22.
- [15] Tegler G, Ericson K, Sorensen J, Bjorck M, Wanhainen A. Inflammation in the walls of asymptomatic abdominal aortic aneurysms is not associated with increased metabolic activity detectable by 18-fluorodeoxyglucose positron-emission tomography. *J Vasc Surg.* 2012;56:802–7.
- [16] Tegler G, Ericson K, Sorensen J, Bjorck M, Wanhainen A. Inflammation in the walls of asymptomatic abdominal aortic aneurysms is not associated with increased metabolic activity detectable by 18-fluorodeoxyglucose positron-emission tomography. *J Vasc Surg.* 2012;56:802–7.
- [17] Tegler G, Sorensen J, Ericson K, Bjorck M, Wanhainen A. 4D-PET/CT with [¹¹C]-PK11195 and [¹¹C]-D-deprenyl does not identify the chronic inflammation in asymptomatic abdominal aortic aneurysms. *Eur J Vasc Endovasc Surg.* 2013;45:351–6.
- [18] CPMP/SWP/2599/02/Rev1. Position Paper on nonclinical safety studies to support clinical trials with a single microdose. European Medicines Agency (EMA), committee for medicinal products for human use (CHMP); 2004. Jun, http://www.emea.europa.eu/pdfs/human/swp/259902_en.pdf.
- [19] Sgouros G. Bone marrow dosimetry for radioimmunotherapy: theoretical considerations. *J Nucl Med.* 1993;34:689–94.
- [20] Corteling R, Wyss D, Trifilieff A. In vivo models of lung neutrophil activation. Comparison of mice and hamsters. *BMC Pharmacol.* 2002. ;2https://doi.org/10.1186/1471-2210-2-1.